Scripta Materialia 273 (2026) 117100

Contents lists available at ScienceDirect

Scripta Materialia

journal homepage: www.journals.elsevier.com/scripta-materialia

Thermoelectric properties of semiconducting approximant crystals in the Al–Ge–Ru system

Yutaka Iwasaki [a,*], Yasuhiro Niwa [b], Koichi Kitahara [c], Kaoru Kimura [d], Ryuji Tamura [b]

[a] National Institute for Materials Science (NIMS) 1-2-1 Sengen, Tsukuba, Ibaraki 305-0047, Japan
[b] Department of Materials Science and Technology, Tokyo University of Science, Tokyo 125-8585, Japan
[c] National Defense Academy, 1-10-20 Hashirimizu, Yokosuka, 239-8686 Kanagawa, Japan
[d] The Institute of Statistical Mathematics, 10-3 Midori-cho, Tachikawa, Tokyo, 190-8562, Japan

ARTICLE INFO

Keywords:
Quasicrystal
Electronic band structure
Intermetallic compounds
Semiconductor compounds
Thermoelectric materials

ABSTRACT

Semiconducting quasicrystals and their approximant crystals (ACs) have attracted significant attention because of their potential applications as thermoelectric materials. Herein, we report the synthesis of a semiconducting AC in the Al–Ge–Ru system and its thermoelectric properties. The Al–Ge–Ru AC exhibited a band gap of approximately 0.25 eV. Notably, we observed a negative Seebeck coefficient, which reached a maximum magnitude of 200 μV K^{-1}, marking the first example of an n-type semiconducting AC. The $Al_{74}Ge_4Ru_{22}$ AC exhibiting degenerate semiconductor behavior reached a dimensionless figure of merit of 0.28 at a peak temperature of 473 K. This represents the highest figure of merit achieved to date for a quasicrystalline-based thermoelectric material.

Thermoelectric materials are capable of converting thermal energy into electrical energy and vice versa. In recent years, with energy and environmental issues becoming increasingly pressing, growing attention has been paid to using thermoelectric materials to generate electricity from waste heat. The performance of thermoelectric materials is evaluated by the dimensionless figure of merit (zT),

$$zT = S^2\sigma T/\kappa, \quad (1)$$

where S, σ, κ, and T represent the Seebeck coefficient, electrical conductivity, thermal conductivity, and the average operating temperature of a sample, respectively. To achieve high zT, materials need to possess a large power factor ($S^2\sigma$) and low κ.

We have focused on quasicrystals as materials that meet the criteria of high $S^2\sigma$ and low κ [1,2]. Quasicrystals exhibit unique properties such as electronic transport [3,4], intermediate valence states [5], unconventional quantum critical states [6], superconductivity [7,8], ferro- and antiferromagnetism [9,10], high-temperature specific heat [11,12], and thermal conductivity [13]. For example, icosahedral quasicrystals found in Al–transition metal systems exhibit electrical properties similar to those of degenerate semiconductors because their electronic structure has a deep pseudogap near the Fermi level. Additionally, quasicrystals exhibit low κ comparable to that of glass because of their complex atomic arrangements, making them a candidate for thermoelectric applications [14]. Takagiwa et al. [15] reported the highest reported zT for quasicrystals of 0.26 at 473 K for the Al–Ga–Pd–Mn system. This value is approximately one fourth of the target for established thermoelectric materials such as $(Bi,Sb)_2Te_3$ [16]. The limited zT of quasicrystals is primarily attributed to their low S of 90 μV K^{-1} compared with 180 μV K^{-1} for $(Bi,Sb)_2Te_3$.

When considering both electron (indicated by subscript e) and hole (indicated by subscript h) contributions, S can be expressed as,

$$S = (\sigma_h S_h - \sigma_e|S_e|)/(\sigma_h+\sigma_e). \quad (2)$$

Eq. (2) implies that the absolute value of S decreases when electrons and holes coexist. Therefore, achieving a large S requires a sufficiently large band gap (E_g). However, despite the discovery of over 70 thermodynamically stable quasicrystals, no semiconducting or insulating quasicrystals have been identified, posing an important unresolved issue in solid-state physics.

The lack of periodicity in quasicrystals makes their band structure difficult to calculate, hindering the search for semiconducting quasicrystals. Therefore, we have explored semiconductor candidates in approximant crystals (ACs) that exhibit quasicrystal-like structures and properties but possess periodicity, enabling band-structure calculations.

* Corresponding author.
E-mail address: IWASAKI.Yutaka@nims.go.jp (Y. Iwasaki).

https://doi.org/10.1016/j.scriptamat.2025.117100
Received 9 July 2025; Received in revised form 15 October 2025; Accepted 8 November 2025
Available online 17 November 2025

The structures of ACs are classified by the degree of approximation represented by two consecutive numbers in the Fibonacci sequence, such as 1/0, 1/1, 2/1, …, q_n/q_{n-1} and therefore, 1/0 ACs have the simplest crystal structure. As a result, we identified Al–Si–Ru 1/0 as the first semiconducting AC [17]. The Al–Si–Ru 1/0 AC has an E_g of 0.15 eV and exhibits a large S of over 200 μV K^{-1} at 350 K, indicating its potential for substantially higher thermoelectric performance compared with that of conventional quasicrystals and their ACs. However, the intrinsic semiconducting nature of Al–Si–Ru 1/0 with low σ limits its maximum zT to 0.03. An attempt has been made to optimize carrier density through Cu doping, but zT of the resulting material only reached a maximum of 0.2 [18]. Semiconducting ACs outside the Al–Si–Ru system have not yet been identified, and guidelines for achieving semiconductor-like band structures in ACs are not well established. Higher performance may be realized by discovering semiconducting ACs in different alloy systems.

Considering the above research context, in this work, we aimed to synthesize novel semiconducting ACs and measure their thermoelectric properties by investigating the Al–Ge–Ru system, in which Si of the Al–Si–Ru system is substituted with another group-14 element, Ge.

We prepared mother ingots by arc melting high-purity raw mixtures of Al(4 N), Ge(4 N), and Ru(3 N) powders under an Ar atmosphere. Raw powder mixtures were prepared by cold pressing. Subsequently, the mother ingots were annealed at 1273 K for 72 to 168 h. Phase identification was conducted using powder X-ray diffraction (XRD) analysis (Smart Lab SE, Rigaku, Japan) and scanning electron microscopy–energy-dispersive spectroscopy analysis (JSM-IT200, JEOL, Japan). Lattice parameters were determined by Le Bail analysis [19] using a partial structure with Rietan-FP software [20]. True density (powder density) was measured using a pycnometer under an He gas atmosphere (AccuPyc 1330 apparatus, Micromeritics, USA).

For the evaluation of thermoelectric properties, specimens were prepared by spark plasma sintering (LABOX-110MC, SinterLand, Inc, Japan), followed by annealing at 1273 K for 72 to 168 h. Density was measured using the Archimedes method, and specific heat and thermal diffusivity were measured using the flash method (LFA 467-HT, Netzsch, German). κ was calculated using measured density, specific heat, and thermal diffusivity. σ was measured using the four-probe method. S was measured using the steady-state temperature difference method (ZEM-3, Advance Riko, Japan). κ, σ, and S were determined in the temperature range from room temperature to 873 K.

The composition of the synthesized Al–Ge–Ru alloys and the results of phase identification are plotted on a ternary phase diagram in Fig. 1.

While there are no reports about Al-Ge-Ru system so far, it was found that a 1/0 AC phase exists near $Al_{74.5}Ge_{3.5}Ru_{22}$. The single-phase region, although having some degree of freedom between Al and Ru, is very narrow. When the Ge content of the alloy exceeds 4.0 at. %, the solubility limit is reached, resulting in a two-phase equilibrium state of the 1/0 AC phase and diamond-structured Ge. Conversely, if the Ge content of the alloy is <3.0 at. %, Ru_4Al_{13} appears as a secondary phase. Additionally, the $RuAl_2$ phase emerges as a secondary phase in the Ru-rich region. In the case of the Al–Si–Ru system, the single-phase region of the 1/0 AC phase is located near $Al_{69}Si_{7.5}Ru_{23.5}$. In contrast, the alloy with composition corresponding to $Al_{69}Ge_{7.5}Ru_{23.5}$ consists of a three-phase equilibrium of the 1/0 AC phase, Ge, and $RuAl_2$. This indicates that the Al–Ge–Ru 1/0 ACs exist in a composition range that is more Al-rich and Ru-poor compared with that of the Al–Si–Ru 1/0 ACs. Furthermore, in the Al–Si–Ru system, multiple ternary compounds [21] exist adjacent to the 1/0 AC phase [22]. Conversely, no ternary compounds exist adjacent to the Al–Ge–Ru AC phase, at least at 1273 K.

Fig. 2 displays the XRD patterns of single-phase samples obtained after arc melting followed by heat treatment at 1273 K for 72 h for the compositions of $Al_{74}Ge_4Ru_{22}$, $Al_{74.5}Ge_{3.5}Ru_{22}$, and $Al_{74}Ge_{3.5}Ru_{22.5}$. Most of the XRD patterns of Al–Ge–Ru 1/0 AC show peaks at similar positions to those calculated for the Al–Si–Ru 1/0 AC, known as the C phase [23], with a lattice constant of approximately 0.77 nm. However, broadening of the peaks on the high-angle side was observed. Additionally, peak splitting appeared at approximately 2θ of 25° and 45° This splitting corresponds to the superlattice peaks that match the 2 × 2 × 2 base-centered superlattice structure of the C phase, known as the C_4 phase, in the Al–Si–Ru 1/0 ACs [23]. Therefore, it is considered that all three samples synthesized this work have the C_4 phase structure. In the Al–Si–Ru system, even within the same 1/0 AC, three phase types exist based on composition: the C phase with primitive cubic lattice, the C_1 phase with a body-centered cubic structure and a 2 × 2 × 2 superlattice structure, and the C_4 phase with a C-centered orthorhombic structure [22]. In contrast, only the C_4 phase was observed in the Al–Ge–Ru system. We prepared two single-phase batches at the same nominal composition. The XRD patterns show slight batch-to-batch differences in peak shapes and relative intensities. Comparable variations are also commonly observed for the same specimen before and after SPS. We attribute these to minute compositional fluctuations, slightly preferred orientation, and small differences in the SPS thermal history. Elucidating the atomic-scale origin will require single-crystal structure analysis, which we plan as future work. Importantly, we have observed similar batch-dependent variations in XRD intensity ratios for related approximants in the Al–Si–Ru and Al–Ir systems, with negligible impact

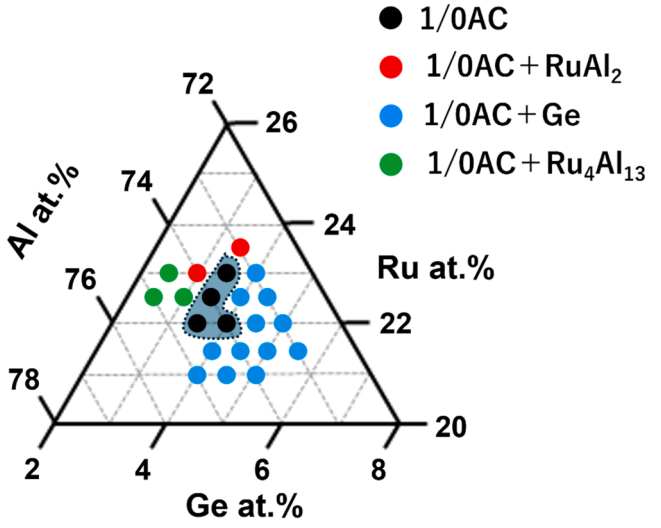

Fig. 1. A ternary isothermal section of the Al–Ge–Ru system near the 1/0 approximant phase at 1273 K.

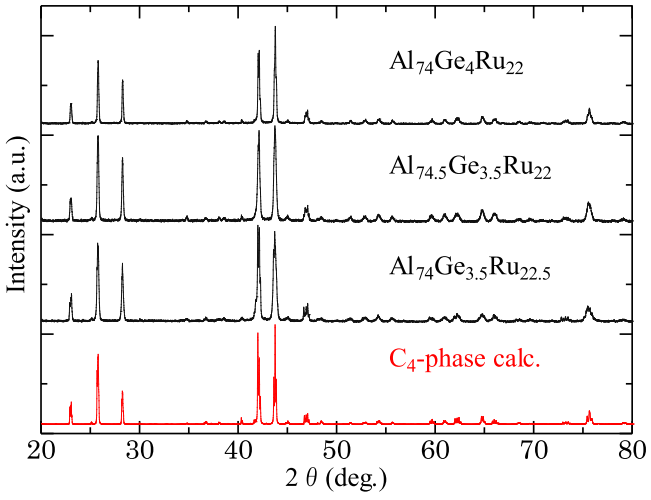

Fig. 2. Powder XRD patterns of single-phase samples in Al–Ge–Ru 1/0 AC with calculated pattern of C_4-phase in the Al–Si–Ru system [23].

on the measured thermoelectric properties.

Table 1 lists lattice constants, unit cell volumes, true densities, relative densities, and the number of atoms per unit cell for the $Al_{74}Ge_{3.5}Ru_{22.5}$, $Al_{74.5}Ge_{3.5}Ru_{22}$, and $Al_{74}Ge_4Ru_{22}$ compositions investigated in this study. The lattice constants were averaged [$a_{ave}=V^{1/3}=(abc)^{1/3}$, where V is the volume of the unit cell and a, b, and c are lattice constants] to give a_{ave} of approximately 1.55 nm, which is twice the lattice constant of the primitive cell of the 1/0 AC, indicating that the Al–Ge–Ru 1/0 AC samples have a 2 × 2 × 2 superlattice structure.

The true density of the synthesized samples is approximately 4.8 g cm^{-3}, which is slightly lower than the 4.9–5.0 g cm^{-3} of the Al–Si–Ru 1/0 ACs. The number of atoms per unit cell calculated using V, the average atomic mass (M_{ave}), and Avogadro's number (N_A) was 246 for both $Al_{74}Ge_{3.5}Ru_{22.5}$ and $Al_{74.5}Ge_{3.5}Ru_{22}$. Considering that the Al–Ge–Ru 1/0 ACs have a superlattice structure with V eight times that of the primitive cell, the number of atoms per primitive cell is 30.8. This is comparable to the number of atoms per unit cell of 31 in the Al–Si–Ru 1/0 ACs.

Fig. 3 shows the temperature dependence of κ for $Al_{74}Ge_{3.5}Ru_{22.5}$, $Al_{74.5}Ge_{3.5}Ru_{22}$, $Al_{74}Ge_4Ru_{22}$, and $Al_{67.6}Si_{8.9}Ru_{23.5}$ [17]. The Al–Ge–Ru 1/0 ACs exhibit quite low κ at room temperature of 1–1.2 W m^{-1} K^{-1} because of the frequent phonon Umklapp scattering caused by their complex crystal structure. The increase of κ with temperature is thought to be caused by the increase of electronic thermal conductivity originating from carrier excitation, which corresponds with the temperature dependence of σ discussed later.

Fig. 4(a) and (b) show the temperature dependence of σ and S, respectively, measured for $Al_{74}Ge_{3.5}Ru_{22.5}$, $Al_{74.5}Ge_{3.5}Ru_{22}$, $Al_{74}Ge_4Ru_{22}$, and $Al_{67.6}Si_{8.9}Ru_{23.5}$ [17]. For all samples, σ increases with temperature above approximately 500 K, whereas each sample shows different temperature dependence of σ near room temperature. The σ values of $Al_{74}Ge_4Ru_{22}$ and $Al_{74.5}Ge_{3.5}Ru_{22}$ exhibit intrinsic semiconducting temperature dependence, increasing exponentially from room temperature. The E_g of $Al_{74}Ge_4Ru_{22}$ estimated from the corresponding Arrhenius plot was 0.25 eV. $Al_{74}Ge_{3.5}Ru_{22.5}$ exhibits degenerate semiconducting temperature dependence of σ, being metallic from room temperature to 423 K, and then showing semiconducting behavior at higher temperatures. These results reveal that Al–Ge–Ru alloys join Al–Si–Ru ones as semiconducting ACs. We note that the band gap of 0.15 eV for Al-Si-Ru 1/0AC, which we previously reported, was not derived from an Arrhenius plot. This value was determined by using the band structure calculated via DFT, with the band gap as a fitting parameter to match the experimental results of the Seebeck coefficient. Although not included in the Al-Si-Ru 1/0AC paper, when the band gap of Al-Si-Ru 1/0AC is calculated using an Arrhenius plot, it ranges from 0.26 to 0.29 eV depending on the sample, which is almost the same as that of Al-Ge-Ru 1/0AC.

The S values of all samples were negative from approximately 300 to 500 K, indicating that the majority carrier was electrons. All samples exhibited absolute S values comparable to those of the Al–Si–Ru 1/0 AC. In particular, $Al_{74.5}Ge_{3.5}Ru_{22}$ and $Al_{74}Ge_4Ru_{22}$ displayed high values of $|S|$ ~200 μV K^{-1} at room temperature. For $Al_{74}Ge_{3.5}Ru_{22.5}$, $|S|$ increases from room temperature to 423 K, reflecting degenerate semiconductor characteristics, which are consistent with the conductivity results. As temperature increases, $|S|$ decreases and approaches zero, suggesting bipolar diffusion arising from the contribution of the minority carrier (holes). Specifically, the sign of S of $Al_{74}Ge_4Ru_{22}$ reverses at approximately 500 K, which is likely because the contribution from hole surpasses that of electrons at high temperature. In contrast, for the nearly intrinsic $Al_{74}Ge_4Ru_{22}$ sample with extremely low σ, this behavior begins near room temperature. In this case, where clear major carriers are absent, the conventional model of bipolar diffusion may not be strictly applicable. The phenomenon is more accurately described as a shift in the transport contribution balance between the few available electrons and holes upon thermal excitation. Such a mechanism can lead to a decrease in $|S|$ from low temperatures, even with a relatively large band gap.

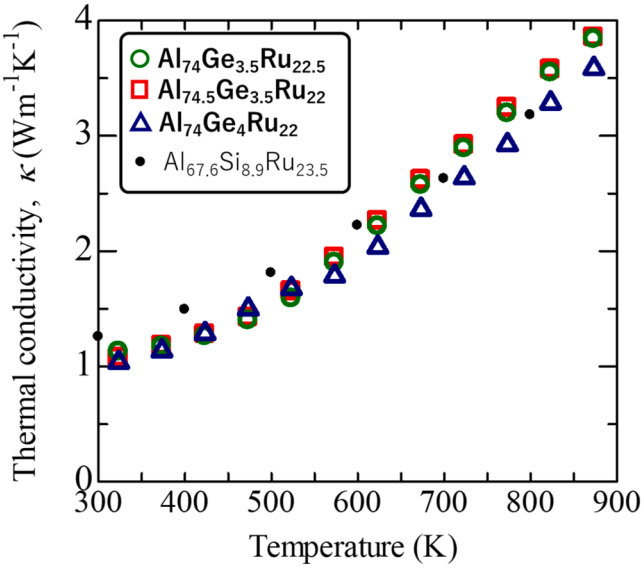

Fig. 3. Temperature dependence of the thermal conductivity κ of Al–Ge–Ru 1/0 and Al–Si–Ru 1/0 ACs.

The Al–Ge–Ru 1/0 ACs obtained in this study show variation of their temperature dependence of σ and S based on composition. This variation is considered to result from shifts of the Fermi level and changes in carrier density as composition changes. The Al–Ge–Ru system 1/0 ACs synthesized in this study all exhibit negative S up to ~500 K, suggesting that the majority carriers are electrons and that the Fermi level is close to the conduction band. In particular, $Al_{74}Ge_4Ru_{22}$ exhibits intrinsic semiconductor properties, indicating that its Fermi level is located near the center of the band gap. Meanwhile, $Al_{74}Ge_{3.5}Ru_{22.5}$ shows temperature dependence of σ akin to that of a degenerate semiconductor, indicating that its Fermi level is positioned close to the conduction band.

Different from the Al–Si–Ru system, the Al–Ge–Ru system exhibits n-type behavior. This is likely related to the Al-rich composition of the Al–Ge–Ru system, which has lower proportions of group-14 elements and Ru compared with the Al–Si–Ru system. The average valence electron count per atom (e/a) of each sample was calculated by assigning valence charges of +3 to Al, +4 to Si and Ge, and −2 to Ru. The e/a values calculated for $Al_{74}Ge_{3.5}Ru_{22.5}$, $Al_{74.5}Ge_{3.5}Ru_{22}$, $Al_{74}Ge_4Ru_{22}$, and $Al_{67.6}Si_{8.9}Ru_{23.5}$ are 1.91, 1.935, 1.94, and 1.914, respectively. For the same structure, a higher e/a generally leads to a greater number of conduction electrons; however, the trends of σ and S do not always correlate with e/a. This is likely caused by differences in the number of atoms within the unit cell for each composition. Elucidating detailed crystal structures through single-crystal XRD could potentially resolve this discrepancy.

Fig. 5(a) shows the temperature dependence of zT for $Al_{74}Ge_{3.5}Ru_{22.5}$, $Al_{74.5}Ge_{3.5}Ru_{22}$, $Al_{74}Ge_4Ru_{22}$, and $Al_{67.6}Si_{8.9}Ru_{23.5}$

Table 1
True density, relative density, lattice constant, volume, and number of atoms per unit cell for Al–Ge–Ru 1/0 ACs, where uncertainty is included in ().

Sample		$Al_{74}Ge_{3.5}Ru_{22.5}$	$Al_{74.5}Ge_{3.5}Ru_{22}$	$Al_{74}Ge_4Ru_{22}$
True density (g cm^{-3})		4.78(8)	4.80(8)	-
Relative density (%)		96.5(0)	97.5(4)	
Lattice constant (nm)	a	1.5467(1)	1.5478(2)	1.54753(7)
	b	1.5579(1)	1.5560(2)	1.55520(7)
	c	1.5503(1)	1.5518(2)	1.55171(7)
Unit cell volume (nm^3)		3.7397(1)	3.7347(9)	3.7291(1)
Atom number per unit cell		246(6)	246(2)	-

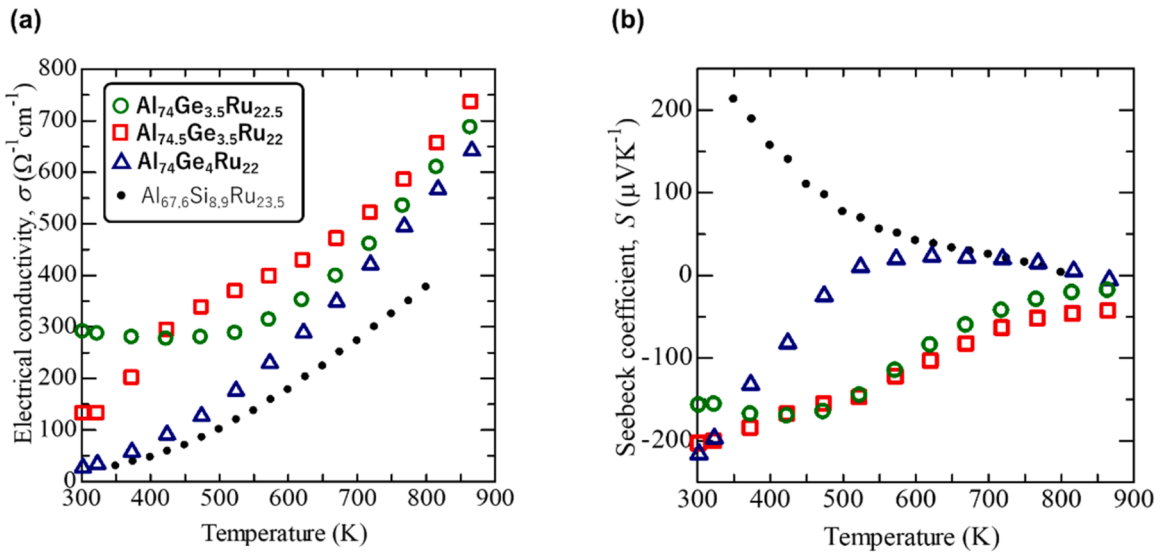

Fig. 4. Temperature dependence of (a) electrical conductivity σ and (b) Seebeck coefficient S in Al–Ge–Ru 1/0 and Al–Si–Ru 1/0 ACs.

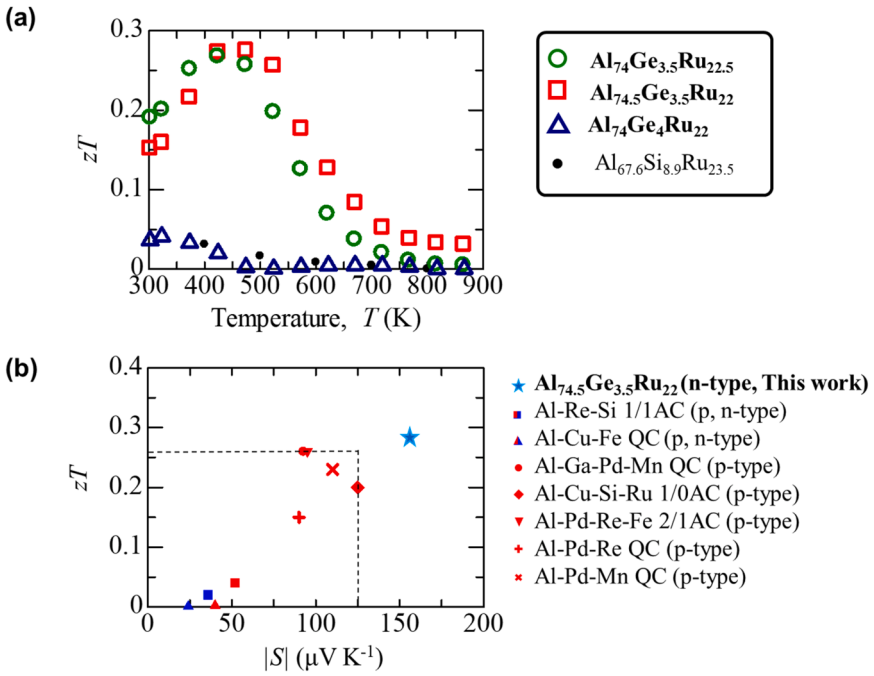

Fig. 5. (a) Temperature dependence of the dimensionless figure of merit zT of Al–Ge–Ru 1/0 and Al–Si–Ru 1/0 ACs and (b) Maximum dimensionless figure of merit zT values obtained in this and previous studies as a function of S.

[17]. Maximum zT values of 0.28 at 473 K, 0.27 at 423 K, and 0.05 at 323 K were obtained for $Al_{74.5}Ge_{3.5}Ru_{22}$, $Al_{74}Ge_{3.5}Ru_{22.5}$, and $Al_{74}Ge_4Ru_{22}$, respectively. The maximum zT of $Al_{74.5}Ge_{3.5}Ru_{22}$ was higher than that of the Al–Si–Ru 1/0 AC because the former possessed a relatively large σ as a result of it behaving as a degenerate semiconductor rather than an intrinsic semiconductor. The maximum zT values obtained in this work and in previous studies on ACs and quasicrystals are presented in Fig. 5(b) as a function of S where zT is maximum. $Al_{74.5}Ge_{3.5}Ru_{22}$ shows both the highest maximum zT and maximum S among reported ACs and quasicrystals [15,18,24–26]. This is attributed to the coexistence of a semiconducting band structure and degenerate semiconducting carrier density in $Al_{74.5}Ge_{3.5}Ru_{22}$. Here, to verify the reliability of the thermoelectric properties, we conducted repeated measurements on a representative sample of $Al_{74.5}Ge_{3.5}Ru_{22}$ which has highest zT among three samples over three times.

The Al–Ge–Ru system was explored with the aim of identifying new semiconducting ACs. Three Al–Ge–Ru 1/0 AC samples, were obtained: $Al_{74}Ge_{3.5}Ru_{22.5}$, $Al_{74.5}Ge_{3.5}Ru_{22}$, and $Al_{74}Ge_4Ru_{22}$. All samples exhibited semiconducting behavior confirming that Al–Ge–Ru 1/0 ACs join Al–Si–Ru 1/0 ones as semiconducting ACs. $Al_{74}Ge_4Ru_{22}$ exhibited an E_g of approximately 0.25 eV and its zT reached 0.28 at 473 K, which is the highest value reported to date for a quasicrystal or AC.

Funding

This work was supported by the Japan Society for the Promotion of Science through Grants-in-Aid for Scientific Research [grant numbers JP19H05817, JP19H05818, JP19K15274, JP23K26367, JP23H01673,

JP24K17495] and the Japan Science and Technology Agency, CREST, Japan [grant number JPMJCR22O3].

CRediT authorship contribution statement

Yutaka Iwasaki: Writing – review & editing, Writing – original draft, Visualization, Supervision, Resources, Investigation, Funding acquisition, Conceptualization. **Yasuhiro Niwa:** Visualization, Validation, Investigation. **Koichi Kitahara:** Validation, Funding acquisition. **Kaoru Kimura:** Validation, Funding acquisition. **Ryuji Tamura:** Validation, Supervision, Resources, Funding acquisition.

Declaration of competing interest

The authors declare no competing financial interest.

Acknowledgments

We thank Natasha Lundin, PhD, from Edanz (https://jp.edanz.com/ac) for editing a draft of this manuscript.

References

[1] D. Shechtman, I. Blech, D. Gratias, J.W. Cahn, Metallic phase with long-range orientational order and no translational symmetry, Phys. Rev. Lett. 53 (1984) 1951–1953.
[2] D. Levine, P.J. Steinhardt, Quasicrystals: a new class of ordered structures, Phys. Rev. Lett. 53 (1984) 2477–2480.
[3] K. Kimura, S. Takeuchi, Experimental studies of electronic transport in quasicrystals, in: D. DiVincenzo, P.J. Steinhardt (Eds.), Quasicrystals: The State of the Art, World Scientific, Singapore, 1999, pp. 325–360.
[4] E.Maciá Barber, Chemical bonding and physical properties in quasicrystals and their related approximant phases: known facts and current perspectives, Appl. Sci. 9 (2019) 2132–2158.
[5] T. Watanuki, S. Kashimoto, D. Kawana, T. Yamazaki, A. Machida, Y. Tanaka, T. J. Sato, Intermediate-valence icosahedral Au-Al-Yb quasicrystal, Phys. Rev. B 86 (2012), 094201-1–094201-6.
[6] K. Deguchi, S. Matsukawa, N.K. Sato, T. Hattori, K. Ishida, H. Takakura, T. Ishimasa, Quantum critical state in a magnetic quasicrystal, Nat. Mater. 11 (2012) 1013–1016.
[7] K. Kamiya, T. Takeuchi, N. Kabeya, N. Wada, T. Ishimasa, A. Ochiai, K. Deguchi, K. Imura, N.K. Sato, Discovery of superconductivity in quasicrystal, Nat. Commun. 9 (2018) 1–8.
[8] Y. Tokumoto, K. Hamano, S. Nakagawa, Y. Kamimura, S. Suzuki, R. Tamura, K. Edagawa, Superconductivity in a van der Waals layered quasicrystal, Nat. Commun. 15 (2024) 1529–1536.
[9] R. Tamura, A. Ishikawa, S. Suzuki, T. Kotajima, Y. Tanaka, T. Seki, N. Shibata, T. Yamada, T. Fujii, C.-W. Wang, M. Avdeev, K. Nawa, D. Okuyama, T.J. Sato, Experimental observation of long-range magnetic order in icosahedral quasicrystals, J. Am. Chem. Soc. 143 (2021) 19938–19944.
[10] R. Tamura, T. Abe, S. Yoshida, Y. Shimozaki, S. Suzuki, A. Ishikawa, F. Labib, M. Avdeev, K. Kinjo, K. Nawa, T.J. Sato, Observation of antiferromagnetic order in a quasicrystal, Nat. Phys. 21 (2025) 974–979.
[11] K. Edagawa, K. Kajiyama, High temperature specific heat of Al–Pd–Mn and Al–Cu–Co quasicrystals, Mater. Sci. Eng. A 294 (2000) 646–649.
[12] Y. Nagai, Y. Iwasaki, K. Kitahara, Y. Takagiwa, K. Kimura, M. Shiga, High-temperature atomic diffusion and specific heat in quasicrystals, Phys. Rev. Lett. 132 (2024), 196301-1–196301-6.
[13] T. Kurono, J. Zhang, Y. Kamimura, K. Edagawa, Large-scale database analysis of anomalous thermal conductivity of quasicrystals and its application to thermal diodes, Sci. Technol. Adv. Mater.:Methods 5 (2025) 1–13.
[14] Y. Takagiwa, K. Kimura, Metallic–covalent bonding conversion and thermoelectric properties of Al-based icosahedral quasicrystals and approximants, Sci. Technol. Adv. Mater. 15 (2014) 044802.
[15] Y. Takagiwa, T. Kamimura, S. Hosoi, J.T. Okada, K. Kimura, Thermoelectric properties of polygrained icosahedral $Al_{71-x}Ga_xPd_{20}Mn_9$ (x=,2,3,4) quasicrystals, J. Appl. Phys. 104 (2008), 073721-1–073721-4.
[16] H.S. Kim, N.A. Heinz, Z.M. Gibbs, Y. Tang, S.D. Kang, G.J. Snyder, High thermoelectric performance in $(Bi_{0.25}Sb_{0.75})_2Te_3$ due to band convergence and improved by carrier concentration control, Mater. Today 20 (2017) 452–459.
[17] Y. Iwasaki, K. Kitahara, K. Kimura, Experimental realization of a semiconducting quasicrystalline approximant in Al-Si-Ru system by band engineering, Phys. Rev. Mater. 3 (2019), 061601-1–061601-5.
[18] Y. Iwasaki, K. Kitahara, K. Kimura, Effects of Cu doping on thermoelectric properties of Al–Si–Ru semiconducting quasicrystalline approximant, Phys. Rev. Mater. 5 (2021), 125401-1–125401-6.
[19] A.Le Bail, Whole powder pattern decomposition methods and applications: a retrospection, Powder Diffr 20 (2005) 316–326.
[20] F. Izumi, K. Momma, Three-dimensional visualization in powder diffraction, Solid State Phenom 130 (2007) 15–20.
[21] K. Kitahara, H. Takakura, Y. Iwasaki, K. Kimura, Crystal structures of five compounds in the aluminium–ruthenium–silicon system, Acta Cryst E79 (2023) 946–951.
[22] K. Kitahara, H. Takakura, Y. Iwasaki, K. Kimura, Phase equilibria in aluminium–ruthenium–silicon system near 1200 kelvin, Mater. Trans. 65 (2023) 18–26.
[23] K. Kitahara, H. Takakura, Y. Iwasaki, K. Kimura, CSD 2287686: experimental crystal structure determination, 2023. (DOI: 10.25505/fiz.icsd.cc2gsjb4).
[24] T. Takeuchi, T. Otagiri, H. Sakagami, T. Kondo, U. Mizutani, H. Sato, Thermoelectric properties of $Al_{82.6-x}re_{17.4}Si_x$ ($7 \leq x \leq 12$) 1/1-cubic approximants, Phys. Rev. B 70 (2004), 144202-1–144202-7.
[25] Y. Takagiwa, T. Kamimura, S. Hosoi, J. Okada, K. Kimura, Thermoelectric properties of Al–Pd–Re quasicrystal sintered by spark plasma sintering (SPS): effect of improvement of microstructure, Z. Kristallogr. 224 (2009) 79–83.
[26] Y. Takagiwa, K. Kimura, Reinvestigation of the thermoelectric properties of Fe-substituted icosahedral Al–Pd–Re quasicrystals, Phys. Status Solidi A 219 (2022), 2200073-1 –2200073-8.